Adaptive Range Oversampling to Achieve Faster Scanning on the National Weather Radar Testbed Phased-Array Radar

CHRISTOPHER D. CURTIS AND SEBASTIÁN M. TORRES

Cooperative Institute for Mesoscale Meteorological Studies, University of Oklahoma, and NOAA/OAR/National Severe Storms Laboratory, Norman, Oklahoma

(Manuscript received 7 December 2010, in final form 8 July 2011)

ABSTRACT

This paper describes a real-time implementation of adaptive range oversampling processing on the National Weather Radar Testbed phased-array radar. It is demonstrated that, compared to conventional matched-filter processing, range oversampling can be used to reduce scan update times by a factor of 2 while producing meteorological data with similar quality. Adaptive range oversampling uses moment-specific transformations to minimize the variance of meteorological variable estimates. An efficient algorithm is introduced that allows for seamless integration with other signal processing functions and reduces the computational burden. Through signal processing, a new dimension is added to the traditional trade-off triangle that includes the variance of estimates, spatial coverage, and update time. That is, by trading an increase in computational complexity, data with higher temporal resolution can be collected and the variance of estimates can be improved without affecting the spatial coverage.

1. Introduction

Range oversampling followed with a whitening (or decorrelation) transformation was originally developed (Torres 2001) with the goal of improving the precision of spectral moment and polarimetric variable estimates on pulsed Doppler weather radars. Range oversampling provides more samples for the estimation of meteorological variables; these samples can be transformed (decorrelated) and efficiently used to reduce the variance of estimates and/or reduce the required observation times (dwell times). Theoretical and simulation studies demonstrating the advantages of these techniques (Torres and Zrnić 2003a,b) have been successfully verified on weather data collected with experimental setups and offline signal processing (Ivić et al. 2003b; Torres and Ivić 2005; Choudhury and Chandrasekar 2007; Hefner and Chandrasekar 2008). However, a real-time implementation of range oversampling processing on weather radars has not been reported to date. Although appealing, a real-time implementation of range oversampling processing may be feasible only on signal processing systems based on modern hardware because of the significantly higher demand for computational power. In this work, we report on a recent real-time implementation of range oversampling techniques that is computationally efficient and leads to faster collection times with little or no sacrifice in data quality.

The need for faster collection times to improve the depiction and understanding of fast-evolving hazardous weather phenomena using radar was recognized over three decades ago (e.g., Miller and Kropfli 1980; Carbone et al. 1985) and has inspired many radar research and demonstration projects (e.g., Wilson et al. 1984; Lin et al. 1986; Qiu and Xu 1996; Wurman 2002; Bluestein and Wakimoto 2003; Zrnić et al. 2007; Heinselman et al. 2008; McLaughlin et al. 2009; Bluestein et al. 2010; Kumjian et al. 2010; Yussouf and Stensrud 2010). Since 2004, scientists at the National Severe Storms Laboratory (NSSL) have been exploring the high-temporal-resolution weather-scanning capabilities of a 10-cm-wavelength, agile-beam, phased-array radar. Located in Norman, Oklahoma, this system is referred to as the National Weather Radar Testbed (NWRT). The interested reader is referred to Zrnić et al. (2007) and Heinselman and Torres (2011) for in-depth technical descriptions of the NWRT hardware and software, respectively. The NWRT is part of the broader multifunction phased-array radar (MPAR) initiative where the use of a single radar system to perform both weather and aircraft surveillance functions

Corresponding author address: Christopher Curtis, 120 David L. Boren Blvd., National Weather Center, Norman, OK 73072.
E-mail: chris.curtis@noaa.gov

DOI: 10.1175/JTECH-D-10-05042.1

is being investigated (Weber et al. 2007; National Academies Press 2008).

A key capability of phased-array radar technology is the high-temporal-resolution sampling that can be achieved through electronic beam steering. Electronic beam steering enables focused observations of different volumetric regions without the delays that are typically associated with mechanically scanned radar beams. However, electronic beam steering does not solve the fundamental scanning trade-off between spatial sampling, update time, and estimate variance.[1] It is through signal processing that range oversampling techniques add a new dimension to this fundamental trade-off. That is, range oversampling can be exploited to reduce dwell times (i.e., faster scanning) without degrading the variance or spatial coverage of meteorological variable estimates.

Even though range oversampling techniques are suitable for radars with reflector antennas, such as the Weather Surveillance Radar-1988 Doppler (WSR-88D), electronically steered phased-array radars are an ideal platform for operational implementation. This is particularly true if the goal is to reduce update times because phased-array radars have no beam smearing or mechanical inertia; thus, they impose no limitations on the radar beam scanning speed. The NWRT obviously meets these criteria, and its digital receiver collects range-oversampled data by default (i.e., it samples at a 60-m spacing with a 240-m pulse). Additionally, the NWRT signal processing cluster is a distributed computing platform, which has more than enough computational power to handle the additional complexity demanded by range oversampling processing.

Motivated by the need for high-temporal resolution data, range oversampling has been running operationally on the NWRT since the spring of 2010. An adaptive algorithm was designed to select processing transformations that lead to lower variances of meteorological variable estimates for varying conditions. The algorithm was tailored for efficiency to ensure compatibility with other required signal processing functions and to minimize the increased requirements for computational power. The real-time implementation of adaptive range oversampling, which is the focus of this work, has led to further reductions of scan update times (up to 2 times) on the NWRT with little or no loss of data quality.

The rest of the paper is organized as follows. Section 2 reviews the theory behind range oversampling processing and motivates the need for an adaptive algorithm. Section 3 describes the real-time implementation of adaptive range oversampling processing on the NWRT. Specifically addressed are the increased computational complexity and the interaction with other signal processing functions. The final section describes the modification of scanning strategies that led to a reduction of update times by exploiting range oversampling processing. The performance improvements are illustrated on weather data collected with the NWRT.

[1] Beam multiplexing (Yu et al. 2007) is purposely ignored in this discussion because its complex sampling renders it incompatible with other signal processing techniques, such as traditional ground clutter filtering.

2. The path to adaptive pseudowhitening

Whereas conventional sampling of weather radar signals (V) occurs at a rate of τ^{-1}, where τ is the duration of the transmitted pulse, range oversampling by a factor of L entails acquiring time series data at increased rates so that L complex samples are collected during the time τ. Thus, range oversampling provides more samples without increasing the dwell time. As mentioned before, oversampling in range is feasible with modern commercial single-board digital receivers (Ivić et al. 2003a). For example, oversampled data are readily available on radar systems that employ software-based digital matched filters, such as the NWRT. On systems that rely on hardware-based digital matched filters, such as the WSR-88D, the hardware has to be reprogrammed to provide oversampled data. Two methods for processing range-oversampled signals are described next: conventional digital matched-filter processing and range oversampling processing. The section on range oversampling processing is further divided to show the progression from the whitening transformation to the currently implemented adaptive pseudowhitening approach.

a. Digital matched-filter processing

A digital matched filter performs coherent averaging of the range-oversampled data from which autocovariances are estimated. Herein, meteorological variable estimates obtained from these autocovariances are referred to as matched-filter-based (MFB) estimates. For an M-pulse dwell and given range resolution cell the corresponding M matched-filtered samples $\mathbf{y}$ are obtained as

$$\mathbf{y} = \mathbf{hV}, \tag{1}$$

where $\mathbf{h}$ is the $1 \times L$ digital matched-filter vector, and $\mathbf{V}$ is the $L \times M$ complex-valued matrix of oversampled time series data. For convenience, we express $\mathbf{V} = (\mathbf{V}_0, \mathbf{V}_1, \ldots, \mathbf{V}_{M-1})$, where $\mathbf{V}_m$ are $L \times 1$ column vectors of range-oversampled signals at sample time m ($m = 0, 1, \ldots, M-1$). That is, $\mathbf{V}_m = [V(0, m), V(1, m), \ldots, V(L-1, m)]^{\mathrm{T}}$, where the superscript T denotes matrix

transposition, and $V(l, m)$ is the signal at the oversampled range index l ($l = 0, 1, \ldots, L - 1$) and sample time m. The digital matched filter that maximizes the signal-to-noise ratio (SNR) of the random signal $\mathbf{V}$ is given by the eigenvector corresponding to the largest eigenvalue of the normalized range correlation matrix $\mathbf{C}_V$(Chiuppesi et al. 1980). The normalized range–correlation matrix can be obtained from the modified pulse, which depends on the transmitter pulse envelope and the receiver impulse response (Torres and Zrnić 2003a).

b. Range oversampling processing

In contrast to the digital matched filter, range oversampling processing performs incoherent averaging of transformed range-oversampled data. Transformed samples are used to compute autocovariance estimates for each oversampled range gate (there are L range gates in each range resolution cell). These autocovariances are averaged in blocks of L estimates from which the meteorological variables are computed. Transformed oversampled signals at a given range resolution cell are obtained as

$$\mathbf{X} = \mathbf{WV}, \tag{2}$$

where $\mathbf{W}$ is the transformation matrix and $\mathbf{X}$ is the transformed time series matrix with the same structure as $\mathbf{V}$. In general, $\mathbf{W}$ can be any $L \times L$ complex-valued matrix that satisfies the ''power-preserving criterion''

$$\mathrm{tr}(\mathbf{W}^*\mathbf{C}_V\mathbf{W}^{\mathrm{T}}) = L, \tag{3}$$

where $\mathrm{tr}(\cdot)$ is the matrix trace operation, the superscript * denotes complex conjugation, and $\mathbf{C}_V$ is the normalized range–correlation matrix.

Estimates obtained from range oversampling processing exhibit lower variances than their MFB counterparts, particularly at high SNR. The variance reduction factor (VRF), defined as the ratio of MFB and range oversampling estimate variances, is useful to quantify the performance of different range oversampling processing transformations. Its value at high SNR, which is denoted by VRF_∞, represents the performance of an oversampling processing transformation in a noise-free environment.

1) WHITENING TRANSFORMATION

A special case of $\mathbf{W}$ is the whitening transformation (Torres and Zrnić 2003a) given by $\mathbf{W} = \mathbf{H}^{-1}$, where $\mathbf{H}$ is the matrix square root of $\mathbf{C}_V$, that is, $\mathbf{C}_V = \mathbf{H}^*\mathbf{H}^{\mathrm{T}}$. Herein, meteorological variable estimates obtained from whitened signals are referred to as whitening transformation–based (WTB) estimates. It can be demonstrated that a whitening transformation produces the maximum VRF_∞ (Torres and Zrnić 2003a). However, a whitening transformation also increases the noise power in the transformed oversampled signal because the noise becomes colored.

The noise-enhancement factor (NEF) is defined as the ratio of the post- to pretransformation noise powers, and it can be expressed in terms of the transformation matrix as [cf. (12) of Torres and Zrnić 2003a]

$$\mathrm{NEF} = \mathrm{tr}(\mathbf{W}^*\mathbf{W}^{\mathrm{T}})/L. \tag{4}$$

The large noise-enhancement factor of the whitening transformation is its main drawback; at low SNR, WTB estimates exhibit larger variances than their MFB counterparts. This effect can be quantified in a more meaningful way by the crossover SNR (SNR_c), which is defined as the SNR at which the variance of estimates obtained with range oversampling and digital matched-filter processing are the same (Torres and Zrnić 2003a). Only at SNRs above SNR_c do estimates from range oversampling processing have a lower variance than those from matched-filter processing.

The effectiveness of range oversampling transformations below and above the SNR_c suggests a straightforward means to mitigate noise enhancement effects. As suggested by Torres and Zrnić (2003a), a simple adaptive technique can use an estimate of the SNR to select the better processing option based on a priori knowledge of SNR_c. That is, range oversampling processing is used at SNRs above SNR_c, and matched-filtering processing otherwise. Hence, the higher the SNR_c, the narrower the range of SNRs for which range oversampling processing adds any value.

2) FIXED PSEUDOWHITENING TRANSFORMATION

As mentioned before, WTB processing achieves maximum variance reduction at high SNR but results in the largest noise enhancement, that is, the highest SNR_c. Unfortunately, if using the simple adaptive algorithm based on SNR_c described above, then the range of effectiveness for whitening is limited. To mitigate this limitation, pseudowhitening (or partial whitening) transformations were recommended by Torres et al. (2004a) as a means to trade less noise enhancement (i.e., a lower SNR_c) for a smaller variance reduction factor at high SNR.

In the general framework of pseudowhitening processing, the transformation matrix is defined as (Torres et al. 2004a)

$$\mathbf{W} = \gamma\mathbf{\Sigma}^{+}\mathbf{P}^{*\mathrm{T}}, \tag{5}$$

where γ is the transformation gain, $\mathbf{\Sigma}^{+}$ is a diagonal real-valued matrix, and $\mathbf{P}$ is a unitary matrix from the singular

value decomposition (SVD) of **H** (defined above as the matrix square root of $\mathbf{C}_V$). From the SVD of **H**, $\mathbf{H} = \mathbf{P}\boldsymbol{\Sigma}\mathbf{Q}^{*\mathrm{T}}$, **P** and **Q** are unitary matrices and $\boldsymbol{\Sigma}$ is a diagonal matrix with the singular values of **H**, σ_l ($l = 0, 1, \ldots, L-1$). The transformation gain γ can be calculated in terms of $\boldsymbol{\Sigma}$ and $\boldsymbol{\Sigma}^+$ in order to satisfy (3) [see Eq. (16) in Torres et al. 2004a] as

$$\gamma = \sqrt{\frac{L}{\mathrm{tr}[(\boldsymbol{\Sigma}^+)^2\boldsymbol{\Sigma}^2]}}. \tag{6}$$

The nonzero entries of $\boldsymbol{\Sigma}^+$ along its main diagonal σ_l^+ determine the type of pseudowhitening transformation. For example, **W** in (5) becomes a whitening transformation if $\sigma_l^+ = \sigma_l^{-1}$. Alternatively, pseudowhitening with a "sharpening" filter is obtained when $\sigma_l^+ = \sigma_l[\alpha\sigma_l^2 + (1-\alpha)]^{-1}$, where α is the sharpening parameter that controls the degree of pseudowhitening (Torres et al. 2004a). As α varies from 0 to 1, **W** ranges from nearly equivalent to a matched filter to a whitening transformation. Herein, meteorological variables obtained using a fixed pseudowhitening transformation are referred to as pseudowhitening transformation–based (PTB) estimates. With this formulation, the NEF defined in (4) becomes

$$\mathrm{NEF} = \frac{\gamma^2}{L}\mathrm{tr}[(\boldsymbol{\Sigma}^+)^2]. \tag{7}$$

Figure 1 shows the standard deviation of signal power estimates as a function of the SNR measured at the output of the digital matched filter. Signal power estimates $\hat{P}$ were obtained with MFB, WTB, and PTB processing of simulated weather signals (Zrnić 1975) with a range oversampling factor of $L = 4$. Statistics were produced from 100 000 realizations of time series data with $M = 12$ samples at the typical NWRT long pulse-repetition time (PRT) of $T_s = 3$ ms and a frequency of $f = 3.2$ GHz. Weather signals were simulated with zero Doppler velocity and 4 m s^{-1} spectrum width. For these conditions, the standard deviations of MFB, PTB ($\alpha = 0.9$), and WTB power estimates at high SNR can be read from the plot as 1.17, 0.68, and 0.62 dB, respectively. Thus, VRF_∞ for PTB and WTB processing (after conversion to linear units) are about 3.4 and 4, respectively. The SNR_c values for PTB and WTB power estimates are about 5 and 10 dB, respectively. As expected, a whitening transformation results in a maximum variance reduction factor of L but the highest SNR_c. Compared to whitening, this specific pseudowhitening transformation based on a sharpening filter with $\alpha = 0.9$ trades a reduction of the SNR_c by a factor of 2 for a 15% smaller VRF_∞.

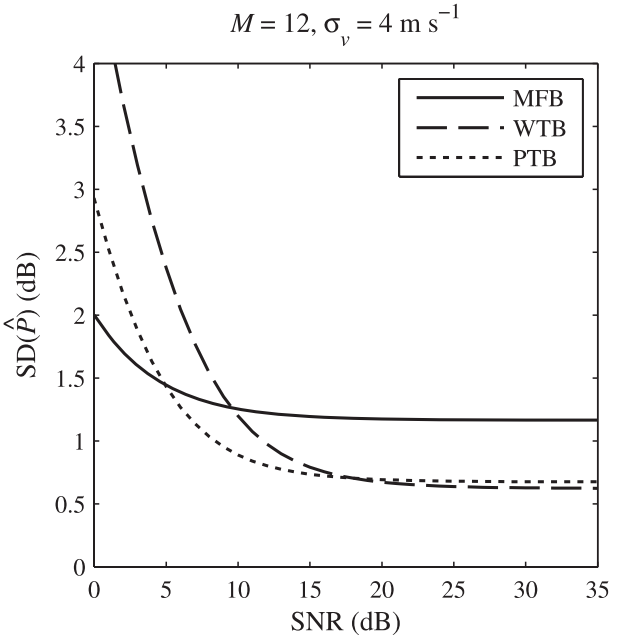

FIG. 1. Standard deviation of MFB, WTB, and PTB signal power estimates as a function of the SNR at the output of the digital matched filter using simulated weather signals with a range oversampling factor of $L = 4$.

Compared to choosing only between MFB and WTB processing, adding PTB processing as a third option helps reduce the estimate variances for intermediate SNRs. For SNRs between 5 and 18 dB, PTB estimates are more precise than both their MFB and WTB counterparts. Still, MFB processing remains the preferred choice at low SNRs (less than 5 dB) and WTB processing is best at high SNRs (more than 18 dB) but only marginally better than PTB processing.

3) Adaptive pseudowhitening transformation

We could proceed by adding more pseudowhitening transformations into the mix; these would lead to more precise estimates within particular SNR intervals. In fact, the best performance would be attained by choosing from an infinite number of pseudowhitening transformations because for every combination of signal parameters (e.g., SNR and normalized spectrum width), there is an optimum pseudowhitening transformation that minimizes the variance of estimates (Torres et al. 2004a). However, optimum performance in terms of minimum variance of estimates is tied to signal characteristics that are not known a priori; hence, the ideal solution involves an adaptive algorithm that dynamically chooses the best pseudowhitening transformation. Such an adaptive pseudowhitening algorithm is discussed next. Herein, meteorological variable estimates obtained using the

TABLE 1. Moment-specific coefficients A, B, C, and D in the generalized expression of the variance of estimates using range-oversampling processing (Torres and Zrnić 2003a). Respectively, S, v, and σ_v denote signal power, Doppler velocity, and spectrum width. SNR_0 is the signal-to-noise ratio at the output of the digital receiver, M is the number of samples in the dwell, L is the oversampling factor, σ_{vn} is the normalized spectrum width ($\sigma_{\mathrm{vn}} = \sigma_v/2v_a$), and v_a is the Nyquist velocity.

	A	B	C	D
S	$\dfrac{1}{2\sigma_{\mathrm{vn}}\pi^{1/2}}$	$\dfrac{2}{\mathrm{SNR}_0}$	$\dfrac{1}{\mathrm{SNR}_0^2}$	$\dfrac{S^2}{ML^2}$
v	$\dfrac{e^{(2\pi\sigma_{\mathrm{vn}})^2}-1}{4\sigma_{\mathrm{vn}}\pi^{1/2}}$	$\dfrac{2\sinh(2\pi\sigma_{\mathrm{vn}})^2}{\mathrm{SNR}_0}$	$\dfrac{e^{(2\pi\sigma_{\mathrm{vn}})^2}}{2\times\mathrm{SNR}_0^2}$	$\dfrac{v_a^2}{\pi^2(M-1)L^2}$
σ_v	$\dfrac{e^{(2\pi\sigma_{\mathrm{vn}})^2}-4e^{(\pi\sigma_{\mathrm{vn}})^2}+3}{4\sigma_{\mathrm{vn}}\pi^{1/2}}$	$\dfrac{2[\cosh(2\pi\sigma_{\mathrm{vn}})^2-1]}{\mathrm{SNR}_0}$	$\dfrac{e^{(2\pi\sigma_{\mathrm{vn}})^2}+2}{2\times\mathrm{SNR}_0^2}$	$\dfrac{v_a^2e^{2(2\pi\sigma_{\mathrm{vn}})^2}}{4\pi^4\sigma_{\mathrm{vn}}^2(M-1)L^2}$

optimum and adaptive pseudowhitening transformations are referred to as optimum pseudowhitening transformation–based (OPTB) and adaptive pseudowhitening transformation–based (APTB) estimates, respectively.

The adaptive pseudowhitening algorithm starts with the previously mentioned optimum pseudowhitening transformation that minimizes the variance of meteorological variable estimates. An expression for the variance of the estimator of a particular spectral moment θ can be computed using Eq. (28) from Torres et al. (2004a),

$$\mathrm{Var}(\hat{\theta}) = D[A\mathrm{tr}(\mathbf{C}_{X_S}^2) + B\mathrm{tr}(\mathbf{C}_{X_S}\mathbf{C}_{X_N}) + C\mathrm{tr}(\mathbf{C}_{X_N}^2)], \tag{8}$$

where A, B, C, and D are moment-specific constants that depend on the SNR at the output of the digital receiver (SNR_0) and the normalized spectrum width (σ_{vn}). The $\mathbf{C}_{X_S}$ and $\mathbf{C}_{X_N}$ matrices are normalized range–correlation matrices of the transformed signal, and noise components of $\mathbf{C}_V$ and can be computed in terms of $\mathbf{W}$ and $\mathbf{H}$ as $\mathbf{C}_{X_S} = \mathbf{W}^*\mathbf{C}_V\mathbf{W}^{\mathrm{T}} = \mathbf{W}^*\mathbf{H}^*\mathbf{H}^{\mathrm{T}}\mathbf{W}^{\mathrm{T}}$ and $\mathbf{C}_{X_N} = \mathbf{W}^*\mathbf{W}^{\mathrm{T}}$ (Torres et al. 2004a). This assumes that the signal and noise components of V are uncorrelated and the noise is white. On the NWRT, signal power (S), mean Doppler velocity (v), and spectrum width (σ_v) are estimated using classical autocovariance processing based on lag-0 and lag-1 autocovariance estimates (Doviak and Zrnić 1993). The variance expression in (8) is exact for the signal power, but is an approximation based on perturbation analyses for the Doppler velocity and spectrum width (Torres and Zrnić 2003b). For these variables, the approximations should be sufficiently accurate even though the resulting transformation may be slightly suboptimal. The values of the constants A, B, C, and D are given in Table 1 for the three previously mentioned spectral moment estimators.

To find the optimal pseudowhitening transformation for a particular variable, the variance expression in (8) is minimized as described in Torres et al. (2004a). This leads to an expression for the transformation [cf. (32) in Torres et al. 2004a] given in terms of the σ_l^+ by

$$\sigma_l^+ = \frac{\sigma_l}{\sqrt{A\sigma_l^4 + B\sigma_l^2 + C}}, \tag{9}$$

where σ_l are the singular values of $\mathbf{H}$. Note that the scaling factor D at the beginning of the generalized variance expression does not appear in the expression for the optimum pseudowhitening transformation. The optimum pseudowhitening transformation is only optimum when SNR and σ_{vn} are known exactly, but these values are not known a priori. In contrast, adaptive pseudowhitening uses estimates of SNR_0 and σ_{vn} to find moment-specific values of A, B, and C needed in (9). We will show that this leads to a nearly optimal transformation that can be implemented in real time.

The first step in adaptive pseudowhitening is to estimate SNR_0 and σ_{vn}. For a straightforward implementation, MFB estimates of SNR_0 and σ_{vn} are computed from matched-filtered samples using the digital matched filter in (1). Because different estimates may be obtained for different range resolution cells, and (9) is specific to each meteorological variable, a new transformation needs to be computed for each spectral moment and each range resolution cell. That is, the MFB estimates of SNR_0 and σ_{vn} are used to calculate moment-specific values of A, B, and C, which are substituted into (9) to find $\mathbf{\Sigma}^+$. Then, at each range resolution cell, a moment-specific transformation $\mathbf{W}$ is formed using (5). Finally, a transformed signal matrix $\mathbf{X}$ is computed for each meteorological variable, which can be used to produce estimates.

Figure 2 illustrates the performance of APTB estimates of signal power compared to MFB, WTB, PTB, and OPTB estimates as a function of the MFB SNR using 100 000 realizations of simulated weather signals with a range oversampling factor of $L = 4$. OPTB estimates are included as a reference; they are only available in a simulation environment because they depend on the precise knowledge of signal parameters. Both plots use

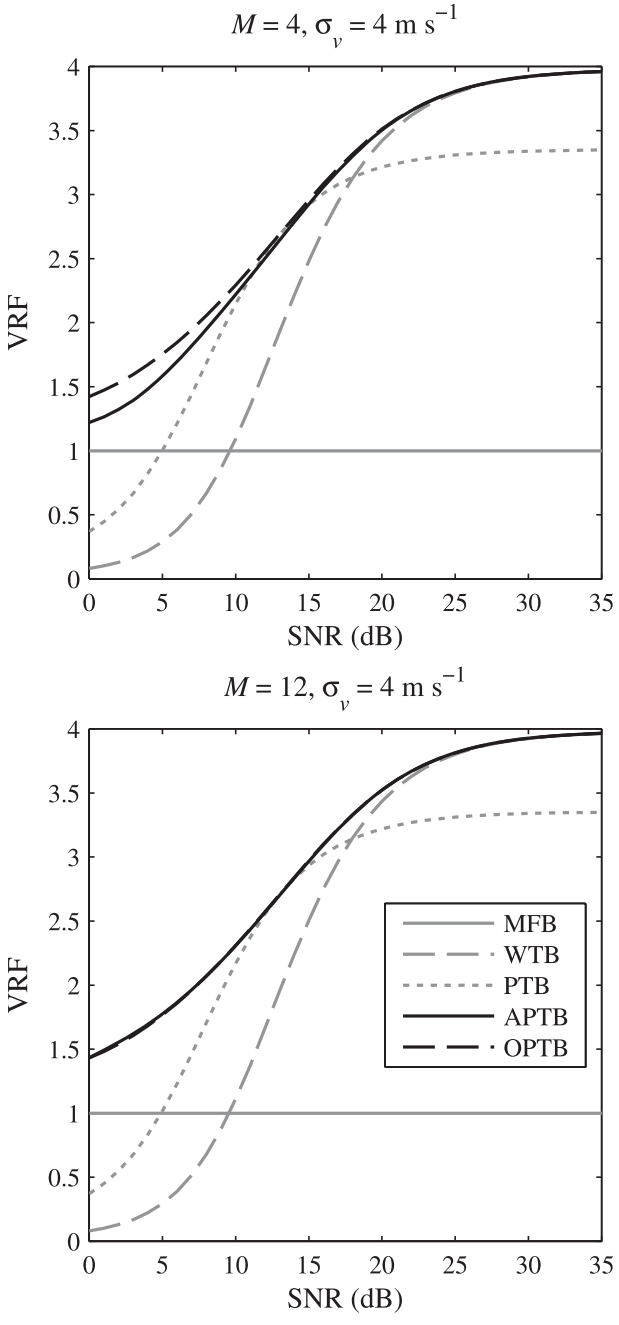

FIG. 2. VRF of MFB, WTB, PTB, APTB, and OPTB signal power estimates as a function of the SNR at the output of the digital matched filter for different number of samples (M) using simulated weather signals with a range oversampling factor of $L = 4$.

the same simulation parameters that were used in Fig. 1, except that $M = 4$ for the top plot and the VRF is displayed for both instead of the standard deviation. As mentioned earlier, the VRF is the ratio of the variance of signal power estimates using MFB processing to the variance of signal power estimates using range oversampling processing. Thus, VRF values greater than one illustrate performance better than the digital matched filter. At high SNRs, theory predicts that WTB processing should reduce the variance by a factor of $L = 4$, which can be clearly seen in both of the plots. Whitening performs well at high SNRs but performs worse than the matched filter at low SNRs, with the same expected SNR_c seen in Fig. 1 of about 10 dB. Similarly, PTB processing underperforms WTB processing at high SNRs, but the SNR_c is reduced to 5 dB. Both APTB and OPTB processing perform as well as WTB processing at high SNRs and better than MFB processing at low SNRs. The difference between the two can be seen when $M = 4$, where OPTB processing outperforms APTB processing at low SNRs. This occurs because the OPTB transformation is computed using the true SNR and σ_{vn}, which are unknown when processing real data, whereas estimates are used to compute the APTB transformation. However, the use of estimates for APTB processing instead of the true values for OPTB processing makes only a small difference at low SNRs. Hence, APTB processing is nearly optimal.

3. Real-time implementation

The main difference between adaptive pseudowhitening and the single transformation processing proposed in previous works is that a meteorological variable–specific transformation is needed at every range resolution cell, which leads to a more complicated real-time implementation. A brute-force approach to adaptive pseudowhitening based on the description from section 2 is presented in this section, but issues with computational complexity and clutter filtering make it less suitable for a real-time implementation. A novel, more efficient approach is then described to address the shortcomings of the brute-force method. The computational complexities of both approaches are compared, and some additional implementation issues are addressed.

a. Brute-force implementation

Even though the brute-force approach was not directly implemented, describing it helps to illustrate the complexities of adaptive pseudowhitening, and it acts as a useful baseline for comparison. The input to the algorithm is the range-oversampled data for a range resolution cell ($\mathbf{V}$), and the outputs are spectral moment estimates. The brute-force steps follow the basic outline given in the previous section:

1) Compute SNR_0 and σ_{vn} from MFB autocovariance estimates computed from $\mathbf{y}$ in (1). Threshold the σ_{vn} value to be above 0.01 and SNR_0 to be above -10 dB.
2) Compute "optimal" moment-specific pseudowhitening transformations $\mathbf{W}(S)$, $\mathbf{W}(v)$, and $\mathbf{W}(\sigma_v)$, using (5),

(6), and (9) for power, velocity, and spectrum width estimates, respectively, where $\mathbf{W}(\theta)$ denotes the transformation specific to the spectral moment θ [as defined in (8)].

3) Transform the original time series matrix $\mathbf{V}$ using the computed moment-specific transformations to produce time series matrices $\mathbf{X}(S)$, $\mathbf{X}(v)$, and $\mathbf{X}(\sigma_v)$ using (2).
4) For each required lag-k autocovariance estimate, compute L range-oversampled moment-specific autocovariances from the corresponding transformed time series matrices $\hat{R}^{(l)}_{X(\theta)}(k) = (M - |k|)^{-1}\sum_{m=0}^{M-|k|-1} X^*(\theta)(l,m)X(\theta)(l,m+k)$. Required autocovariances are lag 0 from $\mathbf{X}(S)$ for power, lag 1 from $\mathbf{X}(v)$ for velocity, and lags 0 and 1 from $\mathbf{X}(\sigma_v)$ for spectrum width.
5) Compute the required autocovariance estimates $\hat{R}_{X(S)}(0)$, $\hat{R}_{X(v)}(1)$, $\hat{R}_{X(\sigma_v)}(0)$, and $\hat{R}_{X(\sigma_v)}(1)$ by averaging the corresponding L range-oversampled autocovariance estimates from step 4.
6) Compute APTB moment estimates from the spectral moment–specific averaged autocovariances.

The first step adds more computational complexity because MFB data need to be produced from $\mathbf{V}$ using a digital matched filter as described in (1). The thresholding of σ_{vn} is necessary to avoid an increase in the variance of all APTB estimators resulting from the large errors of the spectrum width estimator at very narrow spectrum widths. Similarly, thresholding SNR_0 avoids issues with unreasonably small SNR_0 values because of estimation error.

The key part of the brute-force approach that increases computational complexity is step 3. There is a direct computational effect from having a separate matrix of time series data for each meteorological variable and indirect effects associated with ground clutter filtering and other ancillary signal processing functions. It is these indirect effects that may be the most costly because, in some cases, ground clutter filtering could use more floating point operations than all of the other processing steps combined. The major problem is that the brute-force approach can lead to ground clutter filtering of all three matrices of transformed time series data and the MFB data instead of only filtering $\mathbf{V}$. An alternative is to use a ground clutter filter that outputs a filtered version of $\mathbf{V}$ that can then be transformed with moment-specific transformations. This would require either additional computations when using frequency-domain filters[2] or the use of time-domain filters, which may not always be feasible. The preferred approach is to find a way to transform $\mathbf{V}$ in such a way that ground clutter filtering only needs to be applied once and any type of filter can be used.

b. *Efficient implementation*

The novel idea that leads to an efficient real-time implementation is to split up the transformation into two distinct steps. From (5), the first step is the unitary matrix given by $\mathbf{P}^{*\mathrm{T}}$, and the second step is a weighting made up of the gain γ and the diagonal matrix $\mathbf{\Sigma}^{+}$. The unitary matrix is the same for all of the transformations, so $\mathbf{V}$ can be multiplied by $\mathbf{P}^{*\mathrm{T}}$ to give a common partially transformed time series matrix $\tilde{\mathbf{X}} = \mathbf{P}^{*\mathrm{T}}\mathbf{V}$. The weighting $\gamma\mathbf{\Sigma}^{+}$ can then be computed for each meteorological variable and applied separately. If this weighting were applied to the partially transformed time series data, the ground clutter filter would still need to produce a moment-specific filtered version of the time series matrix $\tilde{\mathbf{X}}$ similar to the brute-force approach. The alternative is to apply the weighting step to the autocovariances; this allows nearly any type of filter to be used, including those that produce filtered autocovariances from the Doppler spectrum instead of filtered time series data. That is, the lag-k autocovariance estimate $\hat{R}_X(k)$ from fully transformed data can be computed as the weighted average of the L lag-k autocovariance estimates $\hat{R}^{(l)}_{\tilde{X}}(k)$ from partially transformed data,

$$\hat{R}_X(k) = \sum_{l=0}^{L-1} d_l \hat{R}^{(l)}_{\tilde{X}}(k), \tag{10}$$

where $\mathbf{d} = (d_0, d_1, \ldots, d_{L-1})$ is the length L weight vector. A derivation of the equivalence between the two-step efficient implementation and the brute-force approach given in (10) and the relationship between $\mathbf{d}$ and $\gamma\mathbf{\Sigma}^{+}$ can be found in appendix A.

In addition to the advantages for computing the required autocovariances, the two-step application of the moment-specific adaptive pseudowhitening transformation allows the ground clutter filter to be applied only once, and any filter can be used, including those that produce filtered autocovariances. A further benefit of the efficient implementation concerns matched-filtered data. Both approaches need matched-filtered data in order to estimate SNR_0 and σ_{vn}, but for the efficient implementation, the matched-filtered data are already provided as one of the autocovariances computed from the partially transformed data. This will be explored in more detail as the steps for the efficient implementation are described.

The steps for the efficient implementation are similar to the brute-force approach, but additional improvements simplify the algorithm. For example, with the efficient

[2] In this scenario, conversion back to the time domain after the application of a frequency-domain filter would require L additional Fourier transforms and a way to reconstruct the missing information from the filtered spectral components.

implementation, the two-step process for computing $\mathbf{W}$ using a Cholesky decomposition and an SVD is replaced with a single eigendecomposition. The efficient implementation starts from the normalized range–correlation matrix $\mathbf{C}_V$. An eigendecomposition of the Hermitian matrix $\mathbf{C}_V$ is utilized such that $\mathbf{C}_V = \mathbf{U}^*\mathbf{\Lambda}\mathbf{U}^{\mathrm{T}}$, where $\mathbf{U}$ is the matrix of eigenvectors and $\mathbf{\Lambda}$ is the diagonal matrix of eigenvalues with $\lambda_0 \geq \lambda_1 \geq \cdots \geq \lambda_{L-1} \geq 0$. From the Cholesky decomposition of $\mathbf{C}_V = \mathbf{H}^*\mathbf{H}^{\mathrm{T}}$ and the singular value decomposition of $\mathbf{H} = \mathbf{P}\mathbf{\Sigma}\mathbf{Q}^{*\mathrm{T}}$, it can easily be shown that $\mathbf{U}$ is equal to $\mathbf{P}$ (up to multiplication by unit length complex scalars), and also that $\mathbf{\Lambda} = \mathbf{\Sigma}^2$. Next, the elements of the weight vector $\mathbf{d}$ can be obtained directly from the eigenvalues of $\mathbf{C}_V$. As shown in appendix A, $d_l = g\lambda_l^+$, where g is a power-preserving factor and λ_l^+ are the diagonal entries of $\mathbf{\Lambda}^+ = (\mathbf{\Sigma}^+)^2$. Based on the expression for σ_l^+ given in (9), λ_l^+ can be computed as

$$\lambda_l^+ = (\sigma_l{}^+)^2 = \frac{\lambda_l}{A\lambda_l^2 + B\lambda_l + C}, \tag{11}$$

where the moment-specific A, B, and C values depend on the estimates of SNR_0 and σ_{vn} computed from the matched-filtered autocovariances. The power-preserving factor g can then be computed using the eigenvalues and the equation for γ given in (6) as

$$g = \frac{\gamma^2}{L} = [\mathrm{tr}(\mathbf{\Lambda}^+\mathbf{\Lambda})]^{-1} = \left(\sum_{l=1}^{L}\lambda_l^+\lambda_l\right)^{-1}. \tag{12}$$

From these expressions, the moment-specific weight vectors $\mathbf{d}(S)$, $\mathbf{d}(v)$, and $\mathbf{d}(\sigma_v)$ can be obtained. The last step is to show how the matched-filtered covariances can be computed.

The digital matched filter was described in section 2 as a scaled version of the eigenvector corresponding to the maximum eigenvalue of the normalized range–correlation matrix $\mathbf{C}_V$. The $\mathbf{U}$ (or $\mathbf{P}$) matrix contains the eigenvectors, and the first eigenvector corresponds to the largest eigenvalue. Thus, the first row of $\tilde{\mathbf{X}}$ is the unscaled matched-filtered time series data. If the L autocovariances are computed from $\tilde{\mathbf{X}}$, then $\hat{R}_{\tilde{X}}^{(0)}(k)$ (obtained from the first row of $\tilde{\mathbf{X}}$) is the unscaled, lag-k, matched-filtered autocovariance. The proper scaling factor can be found by treating the matched filter as a pseudowhitening transformation, such that the first row of the transformed data $\mathbf{X}$ is $\mathbf{y}$ from (1) and the other rows are zeros. This is equivalent to selecting a transformation matrix with $\sigma_0^+ = 1$ and $\sigma_l^+ = 0$ for $l = 1, 2, \ldots, L-1$. With this setup and using the fact that $\lambda_l^+ = (\sigma_l^+)^2$, it is easy to see from (12) that the only nonzero element of the weight vector $\mathbf{d}$ is $d_0 = g\lambda_0^+ = \lambda_0^{-1}$; thus, $\hat{R}_{\tilde{X}}^{(0)}(k)/\lambda_0$ is the appropriately scaled matched-filtered autocovariance.

With all of the machinery in place, the steps of the efficient adaptive pseudowhitening algorithm are given next. As with the brute-force approach, the input to the algorithm is the range-oversampled data for a range resolution cell ($\mathbf{V}$), and the outputs are spectral moment estimates.

1) Compute the partially transformed matrix of time series data $\tilde{\mathbf{X}} = \mathbf{U}^{*\mathrm{T}}\mathbf{V}$, using the $\mathbf{U}$ computed from the eigendecomposition of $\mathbf{C}_V$.
2) For each required lag-k autocovariance estimate, compute L range-oversampled autocovariances $\hat{R}_{\tilde{X}}^{(l)}(k)$ from the partially transformed data. Required autocovariances are lags 0 and 1 from $\tilde{\mathbf{X}}$.
3) Compute the MFB estimates of SNR_0 and σ_{vn} from $\hat{R}_{\tilde{X}}^{(0)}(k)/\lambda_0$. Threshold the σ_{vn} value to be above 0.01 and SNR_0 to be above -10 dB.
4) Calculate the nearly optimum moment-specific weight vectors $\mathbf{d}(S)$, $\mathbf{d}(v)$, and $\mathbf{d}(\sigma_v)$ using $d_l(\theta) = g(\theta)\lambda_l^+(\theta)$, (11), and (12).
5) Compute the required autocovariance estimates $\hat{R}_{X(S)}(0)$, $\hat{R}_{X(v)}(1)$, $\hat{R}_{X(\sigma_v)}(0)$, and $\hat{R}_{X(\sigma_v)}(1)$ from $\hat{R}_{\tilde{X}}^{(l)}(0)$, $\hat{R}_{\tilde{X}}^{(l)}(1)$, and the weight vectors from step 4 as shown in (10).
6) Compute APTB spectral moment estimates from the moment-specific averaged autocovariances.

The largest difference between the efficient implementation and the brute-force approach comes in the first few steps. The data are partially transformed in step 1, and any ground clutter filtering can be done between steps 1 and 2 instead of after the moment-specific transformations that are used in the brute-force approach. This greatly simplifies the ground clutter filtering process both in terms of computational complexity and the types of filters that can be effectively utilized. In step 5, the rest of the transformation is applied using the weight vectors computed in step 4.

To summarize, the efficient implementation simplifies the ground clutter filtering process and allows nearly any type of filter to be used, which can reduce the computational complexity significantly. The already filtered MFB data are computed as a by-product of the partial transformation, which is simpler than computing it separately. Our tests show that the efficient implementation takes about 4 times as many computations as digital matched filtering, assuming $L = 4$, while the brute-force implementation takes about 12 times as many computations. This factor of 3 in computational savings is in addition to any savings from ground clutter filtering. A more detailed analysis of the computational complexity can be found in appendix B.

c. Additional implementation issues

The basic steps for performing adaptive pseudowhitening processing have been presented, but there are

a couple of additional issues that need to be addressed for a complete implementation. The first is the effect of these transformations on the noise. The algorithm shows how the autocovariances are computed, but the appropriate noise value needs to be subtracted from the lag-0 autocovariance estimate, or total power, in order to calculate the signal power that is needed in the reflectivity computation. The noise power needs to be adjusted using the NEF from section 2. Although this was introduced as a noise enhancement factor, the factor can be less than 1 and can increase or decrease the noise power depending on the transformation. Based on (7) and using eigenvalues instead of singular values, the moment-specific noise enhancement factor NEF(θ) can be computed for each weight vector as

$$\mathrm{NEF}(\theta) = \sum_{l=0}^{L-1} d_l(\theta). \tag{13}$$

In other words, the NEF is just the sum of the elements of the weight vector. For the MFB case, this reduces to a moment-independent NEF $= \lambda_0^{-1}$. For the APTB case, the signal power can be computed as $\hat{S} = \hat{R}_{X(S)}(0) - \mathrm{NEF}(S)N$, where N is the noise power at the output of the digital receiver and NEF(S) is the signal power–specific noise enhancement factor.

The last issue is data censoring (or thresholding). Data censoring is a data quality issue whereby only data from significant weather returns are utilized (e.g., displayed and sent to algorithms) and data from noise-like returns are not. A common way to censor weather radar data is to use an SNR threshold. Data corresponding to signals above a particular SNR threshold are treated as significant, and data below the threshold are treated either as nonsignificant or noise. For adaptive pseudowhitening, this is complicated by the fact that the noise powers are different for each range resolution cell, and the corresponding SNR threshold should be adjusted because of the lower variance of APTB estimates. For our implementation, we chose a simple approach and used the SNR computed from the MFB data and a fixed threshold. This censors the data in the same way as the matched-filter approach, but the estimates that are designated as significant will often have better quality than the ones computed with the MFB data. By taking advantage of the improved estimates from the APTB processing, it may be possible to preserve more data that are considered significant, but this requires additional research that is beyond the scope of this work.

4. Real data from the NWRT

In spring 2010, the adaptive pseudowhitening algorithm described in the previous section was implemented for real-time operation on the NWRT. The NWRT digital signal processor is a Linux-based distributed-computing system in which a cluster of multiple commercial off-the-shelf dual-processor nodes (based on dual-core 3-GHz Intel Xeon processors) communicate via a high-speed interconnect. All signal processing functions are implemented in software using the concept of processing modes and processing blocks, which maximizes code reusability and leads to a rapid development cycle (Heinselman and Torres 2011). As stated in the introduction, range oversampling techniques can be used to reduce either the variance of estimates or the required observation times. In this section, we use data collected by the NWRT to demonstrate how adaptive pseudowhitening combined with the proper scanning strategy can achieve both faster updates and improved data quality with no loss of coverage. Data are processed to illustrate and compare the performance improvement that was realized after operational NWRT scanning strategies were modified to use adaptive pseudowhitening.

For this example, we will use one of the scanning strategies that was developed for the spring 2010 experiments using conventional matched-filter processing and was later modified to exploit the real-time implementation of adaptive pseudowhitening. The scanning strategy was designed to provide optimized sampling in elevation and azimuth as proposed by Brown et al. (2000) for the WSR-88D. The strategy performs a sequence of elevation scans at 22 unique constant elevations (from 0.5° to 53°). For each elevation scan, the azimuth is step-scanned to cover a 90° azimuthal sector with 109 beams that are spaced at half-beamwidth increments.[3] The PRTs were designed so that their corresponding unambiguous ranges are long enough to sample storms with heights up to 18 km above ground level. ''Split cuts'' (Torres et al. 2004b) are employed at the lower elevation angles (10 elevations below 6°) where long PRTs are needed to meet coverage requirements. At each beam, data collected with a long PRT are used to compute reflectivity estimates with no range ambiguity, and data collected with a short PRT are used to compute Doppler velocity and spectrum width estimates on a larger Nyquist cointerval. These may be ambiguous in range but are ''range unfolded'' using the reflectivity from the long-PRT data. The number of pulses per dwell (beam) depends on the PRT(s) at each elevation angle and is chosen such that the data meet WSR-88D operational standards for data quality (NOAA 2006). For the original NWRT scanning strategy, the total number of beams (2398) and dwell times (determined by the

[3] Beam spacing as a function of beamwidth results in irregular sampling because the beamwidth of phased-array antennas increases as the beam is steered away from boresight.

specific PRTs and number of samples) provide a baseline update time of 118.6 s for the entire sector.

On 2 April 2010, the scanning strategy described above was used on the NWRT to sample a severe storm event southeast of Norman. Figure 3 shows plan-position indicator (PPI) displays of reflectivity (left panels) and Doppler velocity (right panels) fields at ~1054 UTC. Data shown in this figure correspond to the lowest elevation scan at an elevation of 0.5°. At this elevation, 16 samples using the long PRT (3 ms) and 64 samples using the short PRT (0.8 ms) are collected at each range resolution volume. The total dwell time for each beam is 99.2 ms and 10.8 s for the entire elevation scan. The top and middle panels in Fig. 3 correspond to fields obtained with adaptive pseudowhitening and digital matched-filter processing, respectively. Both sets of fields were obtained using the same time series data and the same ancillary processing functions described by Torres et al. (2010), including the novel clutter environment analysis using adaptive processing (CLEAN-AP) algorithm for detection and filtering ground clutter (Warde and Torres 2010) and data censoring. The CLEAN-AP algorithm works well with the efficient implementation because it outputs filtered autocovariances. The panels at the bottom of the figure were obtained with adaptive pseudowhitening processing using simulated shorter dwells that match the modified scanning strategy parameters. The scan time reduction is achieved by collecting only 12 samples with the long PRT and 26 samples with the short PRT. For this example, shorter dwell times are simulated by processing a contiguous subset of the data collected originally at each beam. For the lowest elevation scan, the total dwell time at each beam is 56.8 ms and 6.2 s for the entire elevation scan (~43% shorter than with full-length dwells).

The top and middle panels of Fig. 3 are useful to qualitatively assess the performance of adaptive pseudowhitening processing compared to the standard digital matched-filter processing. The smoother texture of reflectivity and Doppler velocity fields on the same sampling grid (range and azimuthal spacing) is an indication that, as expected, the variance of APTB estimates is smaller than their MFB counterparts when using the same dwell times. Alternatively, comparing the middle and bottom panels of Fig. 3 illustrates the improvements that are realized after the scanning strategy was modified to account for the reduced variances from adaptive pseudowhitening. These images depict the benefit of using adaptive pseudowhitening to reduce update times. Although data in the bottom panels could have been collected in 57% of the original time (if a modified scanning strategy were employed), a texture comparison reveals a small improvement in data quality. Similar dwell-time reductions were applied to all the elevation scans of the scanning strategy, with the greatest time savings attained at the upper elevations (above 6°) where only a single PRT per elevation scan is used. Compared to the original scanning strategy with MFB processing, the modified scanning strategy with APTB processing results in a 46% shorter update time (63.9 s) with little or no loss in data quality and no change in spatial sampling.

Simulations were conducted to quantitatively evaluate the performance improvement that is realized when using the modified scanning strategy in conjunction with adaptive pseudowhitening. Figure 4 shows the variance reduction factor of APTB power and Doppler velocity estimates as a function of the MFB SNR for different spectrum widths. Simulations were run for the same acquisition parameters used in the 0.5° elevation scan of the original and modified scanning strategies (Table 2) and statistics were computed from 100 000 realizations. The VRF was computed between APTB estimates with the modified acquisition parameters and MFB estimates with the original acquisition parameters. Although the total number of samples was reduced by about half, the performance of APTB power estimates using the modified scanning parameters is always better than using original scan parameters and MFB processing in the range of SNRs and spectrum widths depicted in Fig. 4. The trend of the variance reduction curves toward smaller SNRs would indicate crossover points at negative SNRs. However, this is not relevant because only significant power data (SNR $>$ 2 dB) are used in displays and algorithms. On the other hand, APTB Doppler velocity estimates using modified scan settings are only better than the original data for SNRs above 11.3–13.5 dB, depending on the spectrum width. For SNRs less than 11.3–13.5 dB that are also larger than the significant-return SNR threshold for Doppler velocity of 3.5 dB, the new processing and acquisition parameters could result in a variance increase of up to 2 times (an ~40% increase in standard deviation). However, the advantages of higher temporal data resolution and by-and-large improved data quality obtained with the modified scanning strategy outweigh the performance degradation of Doppler velocity estimates at low SNRs.

5. Conclusions

An efficient real-time implementation of adaptive pseudowhitening was employed on the NWRT showing that update times could be reduced by about a factor of 2 compared to conventional matched-filter processing with improved data quality under most conditions. Adaptive pseudowhitening addresses the limitations of whitening at low SNRs by choosing a moment-specific transformation

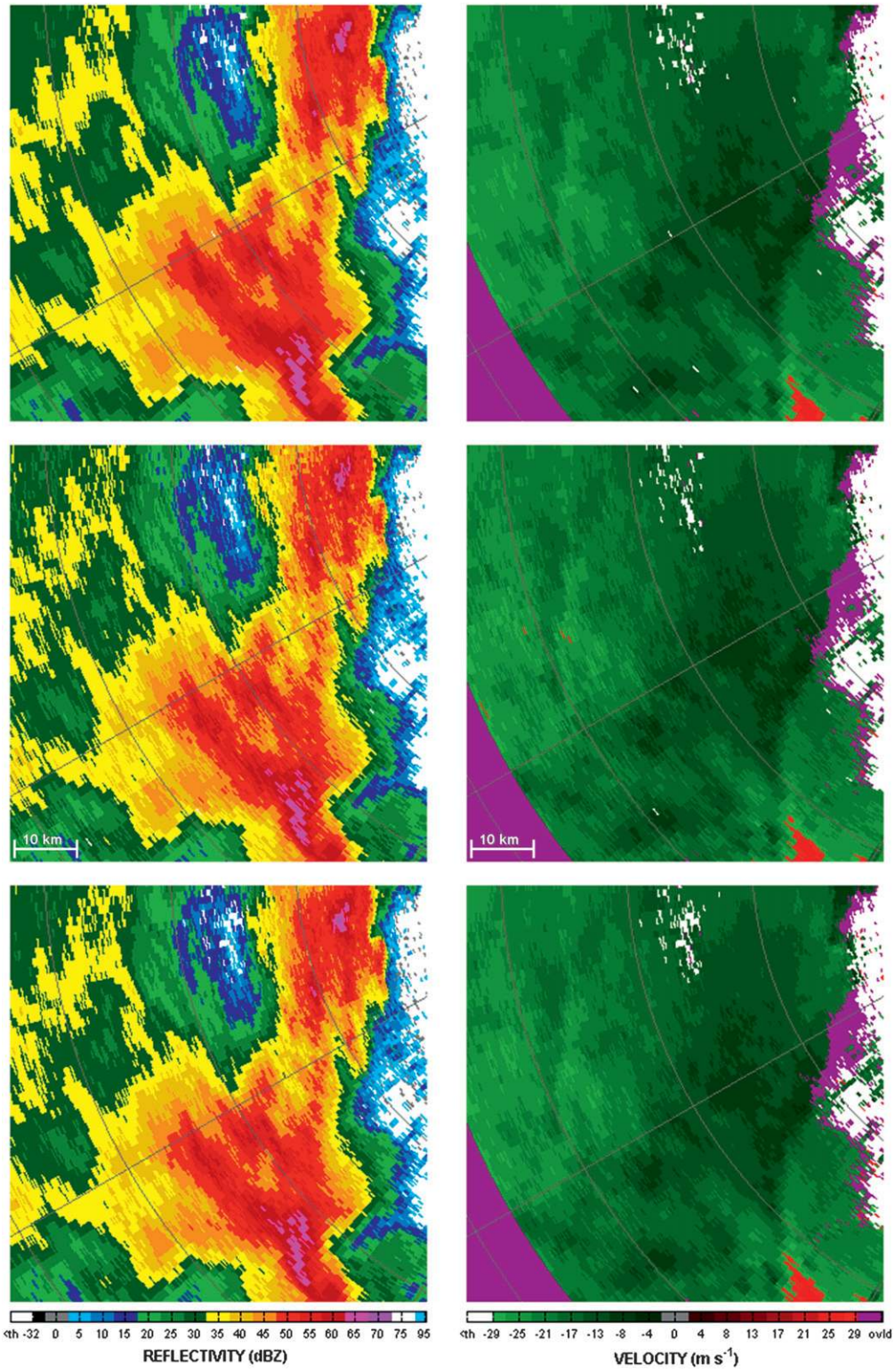

FIG. 3. PPI displays of (left) reflectivity and (right) Doppler velocity fields from data collected with the NWRT at ~1054 UTC 2 Apr 2010. Data are from the 0.5° elevation scan. The original acquisition parameters (long dwells) with (top) adaptive pseudowhitening and (middle) matched-filter processing. (bottom) The (simulated) modified acquisition parameters (short dwells) with adaptive pseudowhitening processing. Acquisition parameters are listed in Table 2.

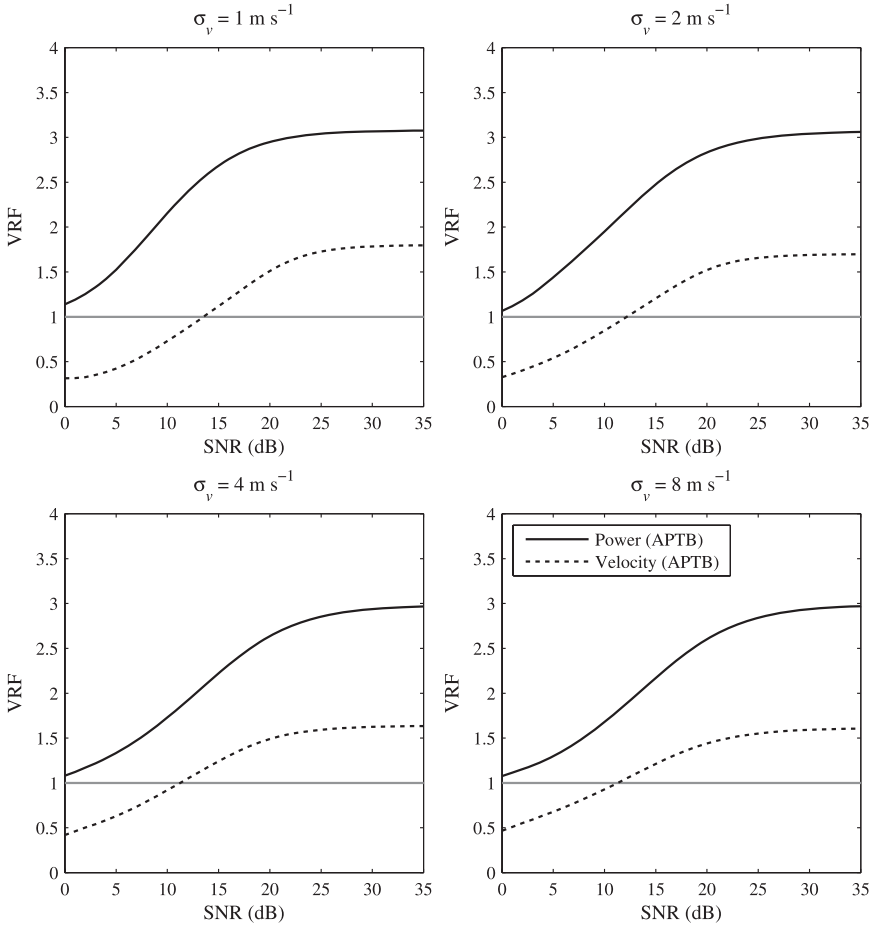

FIG. 4. VRF of APTB power (solid lines) and Doppler velocity (dashed lines) estimates as a function of the MFB SNR for different spectrum widths (1, 2, 4, and 8 m s^{-1}). In each panel, the VRF is computed between APTB estimates using the 0.5° scan with modified (short dwell) acquisition parameters and the MFB estimates using the original (long dwell) acquisition parameters (see Table 2). A gain is realized for VRF > 1; solid gray lines at VRF = 1 represent no gain with respect to the original implementation.

at each range resolution cell that attempts to minimize the variance of the meteorological variable estimators. The transformations are based on the optimal pseudowhitening approach introduced in Torres et al. (2004a), which minimized the expression for the theoretical variance. The variance expression is exact for the signal power, but is an approximation for the Doppler velocity and spectrum width. Unlike optimal pseudowhitening, adaptive pseudowhitening utilizes estimates of the SNR and normalized spectrum width that are substituted for the true values that are unknown. This leads to a nearly optimal real-time algorithm.

Because of drawbacks of the straightforward brute-force approach to adaptive pseudowhitening, an efficient

TABLE 2. Original and modified scanning strategy acquisition parameters for the 0.5° elevation scan (split cut).; M is the number of samples in a dwell and T_s is the PRT. Modified acquisition parameters result in a ~43% shorter scan time for this elevation and an overall ~46% shorter total scan time.

	Original scanning strategy		Modified scanning strategy	
	Long PRT (T_s = 3 ms)	Short PRT (T_s = 0.8 ms)	Long PRT (T_s = 3 ms)	Short PRT (T_s = 0.8 ms)
M	16	64	12	26
Partial dwell time (ms)	48	51.2	36	20.8
Total dwell time (ms)	99.2		56.8	

algorithm was introduced that reduces the computational complexity by a factor of 3 (in the NWRT implementation) along with some other benefits. The main additional benefit is the improvement to the ground clutter filtering process. By splitting the pseudowhitening transformation into two parts, the time series data are only filtered once. In contrast, when using the brute-force approach, either the time series data need to be filtered for each meteorological variable or a very specific type of ground clutter filter needs to be used to produce filtered times series data. This greatly limits the types of filters that can be applied. In addition to more flexibility in ground clutter filtering, the efficient implementation also produces digital matched-filtered time series data as a by-product of the two-part transformation approach. Although the efficient implementation greatly improves on the brute-force approach, the computational requirements are still increased by approximately the oversampling factor compared to digital matched-filter processing. Even though this is a significant increase in computational complexity, the distributed computing platform utilized for the NWRT signal processor allows for this efficient real-time algorithm to be implemented.

To take advantage of the real-time implementation, scanning strategies were modified to reduce scan update times by about a factor of 2. The improvements realized by these modified strategies were illustrated in section 4 using weather data from the NWRT. The modified scanning strategy parameters were selected with the primary goal of obtaining faster updates with overall comparable data quality. Simulations show that these modified strategies combined with adaptive pseudowhitening lead to signal power estimates that are always better than matched-filter processing and yield only slightly degraded performance for Doppler velocity estimates at low SNRs. If the velocity estimates need to be improved in this SNR range, longer update times could be traded for further variance reduction. For example, the dwell times of the modified scanning strategy could be increased until the variance of velocity estimates using adaptive pseudowhitening processing equals that of the matched filter with the original scanning strategy parameters at the usual SNR threshold of 3.5 dB. Nevertheless, in most cases, the advantages of higher temporal resolution and better performance at medium and high SNRs should outweigh the decreased performance at low SNR values.

In the future, this technique could be applied to other radar systems, both those using phased-array antennas and those using reflector antennas (e.g., the WSR-88D). Additionally, this work should be able to be easily extended to the estimation of dual-polarization variables (Torres and Zrnić 2003b; Torres and Ivić 2005). Through signal processing, adaptive pseudowhitening adds a new dimension to the traditional trade-off triangle, which includes variance of estimates, spatial coverage, and update times. By increasing the computational complexity, it is possible to both decrease the update times and improve the variance of estimates without affecting the spatial coverage.

Acknowledgments. The authors thank the anonymous reviewers, Dick Doviak, and Igor Ivić for providing comments to improve the manuscript and also the team of engineers and software developers at NSSL that made the real-time implementation of this technique on the NWRT possible. Funding was provided by NOAA/Office of Oceanic and Atmospheric Research under NOAA-University of Oklahoma Cooperative Agreement NA17RJ1227, U.S. Department of Commerce.

APPENDIX A

Equivalence of Brute-Force and Efficient Adaptive Range Oversampling Implementations

Let $\mathbf{V}$ be the $L \times M$ complex-valued matrix of oversampled time series data, where L is the oversampling factor and M is the number of samples along the sample time. This matrix can be written as $\mathbf{V} = (\mathbf{V}_0, \mathbf{V}_1, \ldots, \mathbf{V}_{M-1})$, where the $\mathbf{V}_m$ are $L \times 1$ column vectors of range-oversampled signals at sample time m. Transformed oversampled signals are obtained as $\mathbf{X} = \mathbf{W}\mathbf{V}$, where $\mathbf{W}$ is the transformation matrix and $\mathbf{X}$ is the transformed time series matrix with the same structure as $\mathbf{V}$. A partial transformation of $\mathbf{V}$ is defined as $\tilde{\mathbf{X}} = \mathbf{P}^{*\mathrm{T}}\mathbf{V}$, where $\mathbf{P}$ is a unitary matrix from the decomposition of $\mathbf{W}$ as $\mathbf{W} = \gamma\boldsymbol{\Sigma}^{+}\mathbf{P}^{*\mathrm{T}}$, where γ is the transformation gain and $\boldsymbol{\Sigma}^{+}$ is a diagonal real-valued matrix.

To see the equivalence between the two-step efficient implementation and the brute-force approach, the autocovariances calculated from the transformed matrix $\mathbf{X}$ can be shown to be identical to appropriately weighting the L autocovariances computed from the rows of the partially transformed matrix $\tilde{\mathbf{X}}$. As described in steps 4 and 5 of the brute-force approach given in section 3, the lag-k autocovariance estimate is obtained as the average of the L range-oversampled autocovariances computed from the rows of $\mathbf{X}$; that is,

$$\hat{R}_X(k) = \frac{1}{L}\sum_{l=0}^{L-1}\hat{R}_X^{(l)}(k) = \frac{1}{L}\sum_{l=0}^{L-1}\left[\frac{1}{M-|k|}\sum_{m=0}^{M-|k|-1}X^{*}(l,m)X(l,m+k)\right]. \tag{A1}$$

This equation can be written in vector form by switching the summation order, combining the constants, and expressing the length L columns of $\mathbf{X}$ as $\mathbf{X}_m = \mathbf{W}\mathbf{V}_m$, where m represents sample time as

$$\hat{R}_X(k) = \frac{1}{(M - |k|)L} \sum_{m=0}^{M-|k|-1} \sum_{l=0}^{L-1} X^*(l,m)X(l,m + k)$$
$$= \frac{1}{(M - |k|)L} \sum_{m=0}^{M-|k|-1} \mathbf{X}_m^{*\mathrm{T}}\mathbf{X}_{m+k}. \quad \text{(A2)}$$

Substituting the expressions for $\mathbf{X}_m$ given previously and the expression for $\mathbf{W}$ from (5), the summation can be rewritten as a weighted dot product,

$$\hat{R}_X(k) = \frac{1}{(M-|k|)L} \sum_{m=0}^{M-|k|-1} (\mathbf{V}_m^{*\mathrm{T}}\boldsymbol{\gamma}\mathbf{P}\boldsymbol{\Sigma}^+)(\boldsymbol{\Sigma}^+\mathbf{P}^{*\mathrm{T}}\boldsymbol{\gamma}\mathbf{V}_{m+k})$$
$$= \frac{1}{(M-|k|)} \sum_{m=0}^{M-|k|-1} (\mathbf{P}^{*\mathrm{T}}\mathbf{V}_m)^{*\mathrm{T}} \frac{(\boldsymbol{\gamma}\boldsymbol{\Sigma}^+)^2}{L} (\mathbf{P}^{*\mathrm{T}}\mathbf{V}_{m+k}). \quad \text{(A3)}$$

The vectors in the summation are the partially transformed columns of $\tilde{\mathbf{X}}$, where $\tilde{\mathbf{X}}_m = \mathbf{P}^{*\mathrm{T}}\mathbf{V}_m$, and the middle expression of the summation is a diagonal matrix $\mathbf{D} = g\boldsymbol{\Lambda}^+ = (\boldsymbol{\gamma}\boldsymbol{\Sigma}^+)^2/L$, which weights the dot product, where $g = \gamma^2/L$ and $\boldsymbol{\Lambda}^+ = (\boldsymbol{\Sigma}^+)^2$. This alternate formulation of the diagonal weighting matrix $\mathbf{D}$ in terms of eigenvalues instead of singular values simplifies the steps of the efficient implementation. With these definitions the previous equation becomes

$$\hat{R}_X(k) = \frac{1}{(M - |k|)} \sum_{m=0}^{M-|k|-1} \mathbf{X}_m^{*\mathrm{T}}\mathbf{D}\tilde{\mathbf{X}}_{m+k}. \quad \text{(A4)}$$

The final step is to replace the weighting from the diagonal matrix $\mathbf{D}$ with an additional summation using a new length L weight vector $\mathbf{d} = (d_0, d_1, \ldots, d_{L-1})$, where $d_l = g\lambda_l^+$, and λ_l^+ is the lth element of the diagonal matrix $\boldsymbol{\Lambda}^+$. This notation for the λ_l^+ was chosen because just as $\boldsymbol{\Sigma}^+$ is based on the singular values of $\mathbf{H}$; the diagonal matrix $\boldsymbol{\Lambda}^+$, and thus the λ_l^+, are based on the eigenvalues of $\mathbf{C}_V$. After replacing the diagonal weighting matrix $\mathbf{D}$ with the new weight vector $\mathbf{d}$, the autocovariance of $\mathbf{X}$ can be written as a double summation similar to the first step in (A2),

$$\hat{R}_X(k) = \frac{1}{M - |k|} \sum_{m=0}^{M-|k|-1} \sum_{l=0}^{L-1} d_l \tilde{X}^*(l,m)\tilde{X}(l,m + k). \quad \text{(A5)}$$

Because $\mathbf{d}$ does not depend on M, the double summation can be rearranged as

$$\hat{R}_X(k) = \sum_{l=0}^{L-1} d_l \left[\frac{1}{M - |k|} \sum_{m=0}^{M-|k|-1} \tilde{X}^*(l,m)\tilde{X}(l,m + k) \right]. \quad \text{(A6)}$$

The final step shows that the autocovariance from $\mathbf{X}$ can be expressed as a weighted sum of L range-oversampled autocovariance estimates $\hat{R}_{\tilde{X}}^{(l)}(k)$, computed from $\tilde{\mathbf{X}}$ as

$$\hat{R}_X(k) = \sum_{l=0}^{L-1} d_l \hat{R}_{\tilde{X}}^{(l)}(k). \quad \text{(A7)}$$

This provides flexibility in computing moment-specific autocovariances by using appropriate choices for the weight vector $\mathbf{d}$.

APPENDIX B

Computational Complexity of Adaptive Range Oversampling

In this appendix, the computational complexity of adaptive range oversampling using the efficient implementation is compared to that of the brute-force implementation and digital matched-filter processing. The following algorithm analyses are not tied to any specific signal processing architecture or clock rate; only the computationally expensive steps are considered to approximately measure the relative complexity of the different implementations.

Assume that a total of E meteorological variable estimates are computed from an $L \times M$ matrix of range-oversampled data, where M is the number of samples along sample time and L is the oversampling factor. For example, $E = 3$ for a typical single-polarization radar (i.e., required variables are signal power, Doppler velocity, and spectrum width), and $E = 6$ for a dual-polarization radar using the simultaneous transmission and reception mode (i.e., required variables are those for a single-polarization radar plus differential reflectivity, differential phase, and magnitude of the cross-correlation coefficient). The number of meteorological variables may vary from the typical values depending on the radar mode (e.g., $E = 1$ for the surveillance mode, whereby only signal power is needed) or depending on specific processing functions [e.g., $E > 3$ when employing multiple spectrum-width estimators as part of the hybrid spectrum-width estimator developed by Meymaris et al. (2009)]. In general, each of these meteorological variables is computed as a function of one or more

TABLE B1. Total number of complex additions and complex multiplications for the brute-force and the efficient implementations of adaptive range oversampling excluding ground clutter filtering and the conventional digital matched-filter processing; M is the number of samples along sample time and L is the range oversampling factor; C_{TOTAL} and C_{LAG} are the numbers of covariance estimators and unique covariance lags to estimate E meteorological variables, respectively.

	Complex additions	Complex multiplications
Adaptive range oversampling, brute-force implementation	$(EL+1)(L-1)M + C_{\mathrm{total}}LM$	$(EL+1+C_{\mathrm{total}})LM$
Adaptive range oversampling, efficient implementation	$(L-1+C_{\mathrm{lags}})LM$	$(L+C_{\mathrm{lags}})LM$
Digital matched-filter processing	$(L-1+C_{\mathrm{lags}})M$	$(L+C_{\mathrm{lags}})M$

covariance estimates (e.g., the Doppler velocity is a function of the lag-1 autocovariance estimate, and the spectrum width is a function of both lag-0 and lag-1 autocovariance estimates). Let C_{total} be the total number of covariance estimates and C_{lags} be the total number of unique covariance lags needed to compute the E meteorological variables For example, for the NWRT PAR implementation $C_{\mathrm{total}} = 4$ (i.e., lag 0 for signal power, lag 1 for Doppler velocity, and lags 0 and 1 for spectrum width) and $C_{\mathrm{lags}} = 2$ (i.e., lags 0 and 1 for the three spectral moments). For a more general result, the computational complexity of the different implementations will be expressed as a function of L, M, E, C_{total}, and C_{lags}.

In the brute-force implementation described in section 3, the computationally expensive steps are (a) digital matched filtering (step 1), (b) oversampled data transformations (step 3), (c) ground clutter filtering, and (d) oversampled covariance computations (step 4). Note that because the meteorological variable estimation process is common to all implementations, it is excluded from the analysis. The digital matched filter in Eq. (1) requires $(L-1)M$ complex additions and LM complex multiplications. Each of the required E oversampled data transformations [see Eq. (2)] requires $L(L-1)M$ complex additions and L^2M complex multiplications. Ground clutter filtering is common to all implementations (but with varying degrees of computational complexity) and will be addressed later. Finally, each of the L oversampled covariance estimates requires $M-k-1$ complex additions and $M-k$ complex multiplications, where k is the covariance lag. Because $M \gg k$, these numbers can be approximated by M. For the implementation on the NWRT PAR, two autocovariance estimates at lag-0 ($k = 0$) and two at lag-1 ($k = 1$) are needed. The total number of complex additions and complex multiplications excluding ground clutter filtering are listed in Table B1.

In the efficient implementation, computationally expensive steps are (a) oversampled data transformation (step 1), (b) ground clutter filtering, and (c) autocovariance estimations (step 2). Basic operations in steps a, b, and c of the efficient implementation require the same number of computations as steps b, c, and d of the brute-force implementation, respectively. However, in the efficient implementation the operations in steps a and b are done only once and the operations in step c are done once for each unique autocovariance lag. For the implementation on the NWRT PAR, lag-0 ($k = 0$) and lag-1 ($k = 1$) autocovariance estimates are needed. Complex additions and complex multiplications are totaled in Table B1.

The computationally expensive steps of conventional digital matched-filter processing are (a) digital matched filtering, (b) ground clutter filtering, and (c) autocovariance estimations. Basic operations in steps a, b, and c require the same number of computations as steps a, c, and d of the brute-force implementation, respectively. However, for digital matched-filter processing the operations in step b are done only once and the operations in step c are done once for each unique autocovariance lag. The total number of complex additions and complex multiplications for digital matched-filter processing are also listed in Table B1 as a reference.

If the ground clutter filter is not applied, the results in Table B1 can be used to estimate the reduction in the number of computations afforded by the efficient implementation as compared to the brute-force approach. Reduction factors for complex additions and multiplications are given by

$$\frac{(EL+1)(L-1)+C_{\mathrm{total}}L}{(L-1+C_{\mathrm{lags}})L} \quad \text{and} \quad \frac{EL+1+C_{\mathrm{total}}}{L+C_{\mathrm{lags}}}, \tag{B1}$$

respectively. Note that these factors are independent of M and roughly simplify to E. Specifically, for the NWRT PAR implementation with $L = 4$, $E = 3$, $C_{\mathrm{total}} = 4$, and $C_{\mathrm{lags}} = 2$, the efficient implementation reduces the number of complex additions and complex multiplications by factors of 2.75 and 2.83, respectively. Both of these factors are very close to the rough estimate of 3.

Table B1 can also be used to assess the increased computational requirements of adaptive range oversampling relative to digital matched-filter processing when the ground clutter filter is not applied. Whereas

the brute-force implementation of adaptive range oversampling requires EL times more complex operations than digital matched-filter processing (12 times more for the NWRT implementation), the efficient implementation only requires an L-fold increase (4 times more for the NWRT implementation).

The computational complexity of the ground clutter filter depends on the specific technique; but it can be argued that it outweighs that of the transformation and estimation steps described above. In fact, the mere estimation of the Doppler spectrum using the periodogram estimator has a computational complexity of $O(M \log M)$ (in big-O notation), and this must be done once for digital matched-filter processing but L times for each transformed oversampled set for either implementation of adaptive range oversampling. Thus, without including any of the additional filtering operations, the number of complex operations for ground clutter filtering dominates compared to the other steps. Hence, it can be used solely as a measure of the computational complexity for the different implementations. Because a spectral ground clutter filter[B1] has to be applied to E sets of transformed oversampled data in the brute-force implementation, it takes E times more complex operations to filter the ground clutter with the brute-force implementation than with the efficient implementation where the filter is applied to one set of transformed oversampled data, and EL times more compared to digital matched-filter processing where the filter is applied just once.

In summary, whether the ground clutter filter is applied or not, the efficient implementation increases the computations by a factor of L compared to digital matched-filter processing, but reduces the number of computations by roughly a factor of E compared to the brute-force approach.

REFERENCES

Bluestein, H. B., and R. M. Wakimoto, 2003: Mobile radar observations of severe convective storms. *Radar and Atmospheric Science: A Collection of Essays in Honor of David Atlas, Meteor. Monogr.,* No. 52, Amer. Meteor. Soc., 105–138.

——, M. M. French, I. PopStefanija, R. T. Bluth, and J. B. Knorr, 2010: A mobile, phased-array Doppler radar for the study of severe convective storms: The MWR-05XP. *Bull. Amer. Meteor. Soc.,* **91,** 579–600.

Brown, R. A., V. T. Wood, and D. Sirmans, 2000: Improved WSR-88D scanning strategies for convective storms. *Wea. Forecasting,* **15,** 208–220.

Carbone, R. E., M. J. Carpenter, and C. D. Burghart, 1985: Doppler radar sampling limitations in convective storms. *J. Atmos. Oceanic Technol.,* **2,** 357–361.

Chiuppesi, F., G. Galati, and P. Lombardi, 1980: Optimisation of rejection filters. *IEE Proc. F Commun. Radar Signal Process.,* **127** (5), 354–360.

Choudhury, S., and V. Chandrasekar, 2007: Wideband reception and processing for dual-polarization radars with dual transmitters. *J. Atmos. Oceanic Technol.,* **24,** 95–101.

Doviak, R. J., and D. S. Zrnić, 1993: *Doppler Radar and Weather Observations*. 2nd ed. Academic Press, 562 pp.

Hefner, E., and V. Chandrasekar, 2008: Whitening dual-polarized weather radar signals with a Hermitian transformation. *IEEE Trans. Geosci. Remote Sens.,* **46,** 2357–2364.

Heinselman, P., and S. Torres, 2011: High-temporal resolution capabilities of the National Weather Radar Testbed phased-array radar. *J. Appl. Meteor. Climatol.,* **50,** 579–593.

——, D. L. Priegnitz, K. L. Manross, T. M. Smith, and R. W. Adams, 2008: Rapid sampling of severe storms by the National Weather Radar Testbed Phased Array Radar. *Wea. Forecasting,* **23,** 808–824.

Ivić, I., A. Zahrai, and D. Zrnić, 2003a: Digital IF receiver—Capabilities, tests, and evaluation. Preprints, *31th Conf. on Radar Meteorology,* Seattle, WA, Amer. Meteor. Soc., 9B.3. [Available online at http://ams.confex.com/ams/pdfpapers/64211.pdf.]

——, D. Zrnić, and S. Torres, 2003b: Whitening in range to improve weather radar spectral moment estimates. Part II: Experimental evaluation. *J. Atmos. Oceanic Technol.,* **20,** 1449–1459.

Kumjian, M. R., A. V. Ryzhkov, V. M. Melnikov, and T. J. Schuur, 2010: Rapid-scan super-resolution observations of a cyclic supercell with a dual-polarization WSR-88D. *Mon. Wea. Rev.,* **138,** 3762–3786.

Lin, Y. J., T. C. Wang, and J. H. Lin, 1986: Pressure and temperature perturbations within a squall-line thunderstorm derived from SESAME dual-Doppler data. *J. Atmos. Sci.,* **43,** 2302–2327.

McLaughlin, D., and Coauthors, 2009: Short-wavelength technology and the potential for distributed networks of small radar systems. *Bull. Amer. Meteor. Soc.,* **90,** 1797–1817.

Meymaris, G., J. Williams, and J. Hubbert, 2009: Performance of a proposed hybrid spectrum width estimator for the NEXRAD ORDA. Preprints, *25th Conf. on Interactive Information and Processing Systems (IIPS) for Meteorology, Oceanography, and Hydrology,* Phoenix, AZ, Amer. Meteor. Soc., 11B.1. [Available online at http://ams.confex.com/ams/pdfpapers/145958.pdf.]

Miller, L. J., and R. A. Kropfli, 1980: Part II: Experimental design and processes. *Bull. Amer. Meteor. Soc.,* **61,** 1173–1177.

National Academies Press, 2008: *Evaluation of the Multifunction Phased Array Radar Planning Process*. National Research Council, 92 pp.

NOAA, 2006: Doppler radar meteorological observations. Part C: WSR-88D products and algorithms. Office of the Federal Coordinator for Meteorological Services and Supporting Research, Federal Meteorological Handbook 11, FCH-H11C-2006, 23 pp.

Qiu, C.-J., and Q. Xu, 1996: Least squares retrieval of microburst winds from single-Doppler radar data. *Mon. Wea. Rev.,* **124,** 1132–1144.

Siggia, A., and J. Passarelli, 2004: Gaussian model adaptive processing (GMAP) for improved ground clutter cancellation and moment calculation. *Proc. Third European Conf. on Radar in Meteorology and Hydrology,* Visby, Gotland, Sweden, ERAD, 67–73.

[B1] Spectral ground clutter filters are common on modern operational radars. For example, the WSR-88D uses the GMAP filter (Siggia and Passarelli 2004), whereas the NWRT PAR uses the CLEAN-AP algorithm (Warde and Torres 2010).

Torres, S., 2001: Estimation of Doppler and polarimetric variables for weather radars. Ph.D. dissertation, University of Oklahoma, 158 pp.

——, and D. Zrnić, 2003a: Whitening in range to improve weather radar spectral moment estimates. Part I: Formulation and simulation. *J. Atmos. Oceanic Technol.,* **20,** 1433–1448.

——, and ——, 2003b: Whitening of signals in range to improve estimates of polarimetric variables. *J. Atmos. Oceanic Technol.,* **20,** 1776–1789.

——, and I. Ivić, 2005: Demonstration of range oversampling techniques on the WSR-88D. Preprints, *32nd Int. Conf. on Radar Meteorology,* Albuquerque, NM, Amer. Meteor. Soc., 4R.5. [Available online at http://ams.confex.com/ams/pdfpapers/96151.pdf.]

——, C. Curtis, and J. R. Cruz, 2004a: Pseudowhitening of weather radar signals to improve spectral moment and polarimetric variable estimates at low signal-to-noise. *IEEE Trans. Geosci. Remote Sens.,* **42,** 941–949.

——, Y. Dubel, and D. Zrnić, 2004b: Design, implementation, and demonstration of a staggered PRT algorithm for the WSR-88D. *J. Atmos. Oceanic Technol.,* **21,** 1389–1399.

——, C. Curtis, I. Ivić, D. Warde, E. Forren, J. Thompson, D. Priegnitz, and R. Adams, 2010: Update on signal processing upgrades for the National Weather Radar Testbed. Preprints, *26th Int. Conf. on Interactive Information and Processing Systems (IIPS) for Meteorology, Oceanography, and Hydrology,* Atlanta, GA, Amer. Meteor. Soc., 14B.2. [Available online at http://ams.confex.com/ams/pdfpapers/163745.pdf.]

Warde, D., and S. Torres, 2010: Automated real-time mitigation of ground clutter contamination for Doppler weather radars. Preprints, *Sixth European Conf. on Radar Meteorology and Hydrology (ERAD),* Sibiu, Romania, Romanian National Meteorological Administration, P2.10. [Available online at http://www.erad2010.org/pdf/POSTER/02_Advances/10_ERAD2010_0349_s.pdf.]

Weber, M. E., J. Y. N. Cho, J. S. Herd, J. M. Flavin, W. E. Benner, and G. S. Torok, 2007: The next-generation multimission U.S. surveillance radar network. *Bull. Amer. Meteor. Soc.,* **88,** 1739–1751.

Wilson, J. W., R. D. Roberts, C. Kessinger, and J. McCarthy, 1984: Microburst wind structure and evaluation of Doppler radar for airport wind shear detection. *J. Climate Appl. Meteor.,* **23,** 898–915.

Wurman, J., 2002: The multiple-vortex structure of a tornado. *Wea. Forecasting,* **17,** 473–505.

Yu, T.-Y., M. B. Orescanin, C. D. Curtis, D. S. Zrnić, and D. E. Forsyth, 2007: Beam multiplexing using the phased-array weather radar. *J. Atmos. Oceanic Technol.,* **24,** 616–626.

Yussouf, N., and D. J. Stensrud, 2010: Impact of phased-array radar observations over a short assimilation period: Observing system simulation experiments using an ensemble Kalman filter. *Mon. Wea. Rev.,* **138,** 517–538.

Zrnić, D. S., 1975: Simulation of weatherlike Doppler spectra and signals. *J. Appl. Meteor.,* **14,** 619–620.

——, and Coauthors, 2007: Agile beam phased array radar for weather observations. *Bull. Amer. Meteor. Soc.,* **88,** 1753–1766.